Effective Sparse Recovery Framework for Ultra-Wideband Robust Plane Wave Generator

Wang, Heng; Wang, Weiming; Wu, Yongle; tang, bihua; song, xiumin; Liu, Yuanan; Pedersen, Gert Frølund; Fan, Wei

Published in:
IEEE Antennas and Wireless Propagation Letters

DOI (link to publication from Publisher):
10.1109/LAWP.2022.3215582

Publication date:
2022

Effective Sparse Recovery Framework for Ultra-Wideband Robust Plane Wave Generator

Heng Wang, Weimin Wang, *Senior Member, IEEE,* Yongle Wu, *Senior Member, IEEE,* Bihua Tang, Xiumin Song, Yuanan Liu, *Member, IEEE,* Gert Frølund Pedersen *Senior Member, IEEE* and Wei Fan, *Senior Member, IEEE,*

***Abstract*—This letter proposes a novel ultra-wideband plane wave generator (PWG) design methodology suitable for a low-cost small anechoic chamber. Several novel strategies are proposed to handle various crucial concerns in practice to make the proposed methodology reliable and robust. Specifically, the sub-array-based amplitude-only excitation method is capable of reducing the required number of control channels without the need for phase shifters, which can significantly simplify the feeding network complexity. One major concern of the PWG application is the non-negligible multipath reflections in small anechoic chambers. Thus, a novel regression approach, imposing the constraint of maximum energy outside the quiet zone (QZ), is implemented to suppress the reflection level. For the design of the PWG layout, a compressed sensing-based adaptive backtracking orthogonal matching pursuit (ABOMP) algorithm is proposed. In the simulation, a spherical test zone supporting the ultra-wideband frequency over 2.4-5 GHz is synthesized with the proposed methodology, and the effectiveness and robustness are comprehensively investigated.**

***Index Terms*—Antenna measurement, constrained regression, compressed sensing, plane wave generator.**

I. Introduction

HIGHLY integrated active antenna system (AAS) will no longer provide any connected radio frequency (RF) port for testing, entailing the cost-effective over-the-air (OTA) interface testing solution in urgent demand [1-3]. The antennas under test (AUT) are expected to be measured under the ideal plane wave illuminations, and the test zone shall be wideband and large enough to support various sizes of communication devices, especially the sub-6 GHz massive Multiple-Input Multiple-Output (MIMO) base stations (BSs) [4]. Plane wave generator (PWG) has been developed and discussed for many years and was permitted for the AAS OTA conformance testing by the 3GPP organization [5].

The basic principle of PWG is to coherently synthesize the plane wave field in the quiet zone (QZ) via properly allocating excitations for the contained antennas. Various methodologies, e.g., in [6-12], have been developed to determine the optimal locations and excitations of PWG antennas for a high-quality and cost-effective plane wave synthesis. For example, a systematic guideline on the PWG geometrical design and the stability of the solution are studied in [9]. Applying the sparse representation theory, [10] proposed a novel PWG design method with fewer radiating sources. Most of them, however, are limited to narrowband applications and require rigorous amplitude and phase feeding control, except for the tapering methods [11]. However, it is typically applied for the PWG with a large aperture and is not ideal for the small anechoic chambers [8]. In addition, although several commercial PWG systems have been reported in recent years [12], the design details were not given. This letter aims to propose a novel methodology to derive the geometrical layout and the excitation coefficients for the wideband PWG suitable in a small anechoic chamber for the sub-6 GHz scenarios, where the chamber dimension is the dominant cost factor.

Compressed sensing has been widely utilized in various engineering fields of research [13-15] and is employed to determine a sparse PWG array in this letter. The sparse recovery generally results in non-uniform arrays, and such arrangements are demonstrated to support ultra-wideband PWG performance [8] and reduce array truncation effects [17]. Furthermore, this strategy effectively reduces the number of required antenna elements, reducing the cost of the PWG system. Different from the conventional amplitude and phase control for each PWG element in the feeding network, the amplitude-only excitation method (i.e., with the same phase excitation for all PWG elements) and the sub-array excitation principle (i.e., without the need for individually exciting each PWG elements) are adopted in this letter, significantly reducing the number of required excitation channels and the feeding network complexity. It is crucial since the individual excitation method is rather complicated and cost-prohibitive for wideband applications [12]. Furthermore, a novel constrained regression approach is proposed for excitation computation. This strategy could suppress the energy outside the QZ and enable the stable generated field inside the QZ in small anechoic chambers.

Notations: $\lfloor x \rfloor$ is to calculate the integer part of x. $(\cdot)^T$,$(\cdot)^H$, $\|\cdot\|_p$, and $\|\cdot\|_\infty$ are the transpose, Hermitian transpose, p-norm, and infinity norm operations, respectively.

II. Problem Formulation

The PWG configuration, generating a spherical test zone with the diameter of D_Q, is shown in Fig. 1, and all the antenna elements with the same digital label, i.e., located on the same concentric circle, are considered as a sub-array. A two-dimensional circular QZ with a diameter of D_Q is defined for algorithm implementation. The center of PWG is

This work was supported by The National Key Research and Development Program of China (No. 2022YFF0604300). The BUPT Excellent Ph.D. Students Foundation (No. CX2021216).

Heng Wang, Weimin Wang, Yongle Wu, Bihua Tang, and Yuanan Liu are with Beijing University of Posts and Telecommunications, Beijing, 100876, China.

Gert Frølund Pedersen and Wei Fan are with Department of Electronic Systems, Aalborg University, 9220 Aalborg, Denmark.

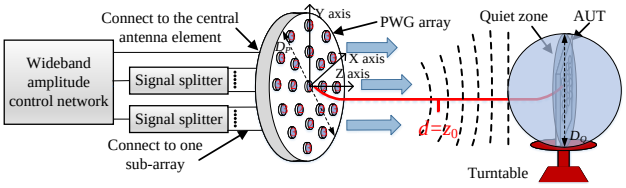

Fig. 1. An illustration of the PWG system configuration.

considered as the origin of the coordinate system, and the QZ is centered at the Z-axis. The distance between the PWG and the QZ is $d = z_0$. The diameter of the PWG aperture is D_P.

A. General System Model

Let us consider a PWG composed of U sub-arrays, and the uth sub-array contains L_u radiating elements. With the coherent superposition of the electromagnetic waves radiated from the sub-arrays of PWG, the generated field in the QZ can be expressed as: $\boldsymbol{T} = \mathbf{H}\boldsymbol{G}$, where $\boldsymbol{T} \in \mathbb{C}^{M\times 1}$ is the vector containing the generated complex field values of the M sampling points in the QZ. $\mathbf{H} = [\boldsymbol{h}_1, ...\boldsymbol{h}_U] \in \mathbb{C}^{M\times U}$ is the polarized transfer matrix. $\boldsymbol{h}_u = [h_{1,u}, ...h_{M,u}]^T \in \mathbb{C}^{M\times 1}$ is the uth column vector of $\mathbf{H}$. $h_{m,u}$ represents the coherent sum of the transfer coefficients from the L_u elements of the uth sub-array to the mth sampling point in the QZ. $\boldsymbol{G} \in \mathbb{C}^{U\times 1}$ is the vector of real number excitations for the U sub-arrays. The objective function to obtain the excitation vector is:

$$\min_{\boldsymbol{G}} \| \mathbf{H}\boldsymbol{G} - \boldsymbol{e}\cdot\exp(j\phi)\|_2. \tag{1}$$

$\boldsymbol{e} = [1, ..., 1]^T \in \mathbb{C}^{M\times 1}$ and ϕ is the phase of the target field. Note that we are concerned with the uniformity of the generated field, while the field phase value ϕ is not important. Obviously, the calculated amplitude-only excitation vector $\boldsymbol{G}$ varies when different ϕ values are set for $\boldsymbol{e}$ in regression, resulting in different synthesized fields. We should therefore find the optimal phase value ϕ^{opt} and optimal excitation $\boldsymbol{G}^{opt}$ minimizing the field deviations, and the phase term $\exp(j\phi)$ can be moved to the PWG side:

$$\underset{\phi^{opt},\boldsymbol{G}^{opt}}{inf}\left\{ f(\mathbf{H}\cdot\exp(-j\phi)\boldsymbol{G}) \,\middle|\, \min_{\boldsymbol{G}} \| \mathbf{H}\cdot\exp(-j\phi)\boldsymbol{G} - \boldsymbol{e}\|_2 \right\}, \tag{2}$$

where $inf(S)$ denotes the infimum of the subset S. $f(\cdot)$ is a metric measuring the synthesized field deviation defined as :

$$f(\boldsymbol{T}) = 20log_{10}(\frac{\alpha_{max}}{\alpha_{min}}) + \varepsilon(\frac{180\cdot|\psi_{max} - \psi_{min}|}{\pi}) \tag{3}$$

α_{max} and α_{min} are the maximum and minimum amplitude in the QZ, respectively, while ψ_{max} and ψ_{min} are the maximum and minimum phases in the QZ, respectively. ε is a scaling factor set to 0.1 in this work and can be flexibly adjusted according to the performance requirements [8].

B. Constrained Regression

A penalty function in [10] is proposed to mitigate the unwanted energy outside the QZ. It is a competent choice in narrowband, but the parameters should be adjusted for wideband scenarios. In this letter, we proposed a novel constrained regression strategy. The basic idea is that if the maximum energy outside the QZ is lower than a threshold δ_{thr}, electromagnetic reflections caused by the imperfect absorber in the small anechoic chamber can be mitigated. (1) can be rewritten with a non-linear constraint:

$$\begin{aligned} &\min_{\boldsymbol{G}} \| \mathbf{H}\cdot\exp(j\phi)\boldsymbol{G} - \boldsymbol{e}\|_2 \\ &\text{s.t.} \quad \| \mathbf{H}'\cdot\exp(j\phi)\boldsymbol{G}\|_\infty < \delta_{thr} \end{aligned} \tag{4}$$

Where $\mathbf{H}'$ is the transfer matrix between the PWG sub-arrays and the zone (with the aperture of D_O) outside the QZ. To solve (4), a logarithmic barrier function can be introduced. (4) can be written as:

$$\min_{\boldsymbol{G}} \left\{ \begin{array}{r} \| \mathbf{H}\cdot\exp(j\phi)\boldsymbol{G} - \boldsymbol{e}\|_2 \\ -(1/t)log(\delta_{thr} - \| \mathbf{H}'\cdot\exp(j\phi)\boldsymbol{G}\|_p) \end{array} \right\} \begin{array}{l} t > 0, \\ p \gg 0. \end{array} \tag{5}$$

(5) can be solved via the quasi-Newton method [18], where t and p are hyper-parameter. Specifically, the convex optimization can be performed for (1) with the preset ϕ. The obtained excitation will be used as the initial values in the quasi-Newton method to calculate the final optimal amplitude excitations. Then ϕ is reset, and we repeat this procedure until all possible phase values are traversed. $\boldsymbol{G}^{opt}$ can then be obtained. Note that ϕ^{opt} is only used to calculate $\boldsymbol{G}^{opt}$, and we do not have to set it in practical PWG. It should be stressed that the transfer matrices $\mathbf{H}$ and $\mathbf{H}'$, phase term ϕ for computation needs, and excitation coefficients $\boldsymbol{G}$ are frequency dependent, and the optimal excitation coefficients $\boldsymbol{G}^{opt}$ are determined with different values at different frequencies.

C. Sparse Recovery for PWG Layout

The sparse recovery for the sub-array-based PWG is a 0-norm minimization problem and is, therefore, NP-hard [13]. In [11], a brute force method is adopted. However, the optimal number of antennas in each sub-array is typically unknown. For this reason, combined with the above theories, a legible adaptive backtracking orthogonal matching pursuit (ABOMP) approach for the sparse PWG design is derived.

1) Over-complete dictionary construction: Regarding the candidate PWG sub-array, we first define $\hat{r}_s$ and $\Delta\hat{r}$ as starting radius and radius interval, respectively. The number of candidate sub-arrays can be characterized as: $\hat{U} = \lfloor(D_P/2 - \hat{r}_s)/\Delta r_s\rfloor + 1$. For the $\hat{u}$th candidate sub-array, its radius is: $\hat{r}_{\hat{u}} = \hat{r}_s + (\hat{u}-1)\cdot\Delta\hat{r}$, $\hat{u} = 1, ..., \hat{U}$. Since the number of radiating elements contained in a candidate sub-array is quite problematic to be determined, we applied the non-redundant sampling strategy [6] to determine the number of antennas contained in each candidate sub-array. Specifically, there should be $\hat{L}_{\hat{u}} = 2M_{\hat{u}} + 1$ antennas uniformly deployed on the $\hat{u}$th concentric circle candidate sub-array with the radius of $\hat{r}_{\hat{u}}$ [6] [10]. $M_{\hat{u}} = \lfloor\pi D_Q\chi_1^\star\sin(\theta_n)/\lambda_b\rfloor$, where $\chi_1^\star = 1 + (\chi_1 - 1)\sin(\theta_n)^{-2/3}$, and $\theta_n = \tan^{-1}(\hat{r}_{\hat{u}}/z_0)$. λ_b is the wavelength of the lowest frequency of the designed wideband. χ_1 is an adjustable parameter. The possible numbers of antennas on the $\hat{u}$th candidate sub-array can therefore be derived with different χ_1 values. To construct an over-complete dictionary, we preset a small χ_1 value as χ_1^s and a large χ_1 value as χ_1^l to derive the minimum $\hat{L}_{\hat{u}}^{min}$ and

maximum $\hat{L}_{\hat{u}}^{max}$ numbers of antennas in the $\hat{u}$th candidate sub-array. Thus $\hat{L}_{\hat{u}}$ can be the integer ranging from $\hat{L}_{\hat{u}}^{min}$ to $\hat{L}_{\hat{u}}^{max}$. In other words, there are $\hat{L}_{\hat{u}}^{max} - \hat{L}_{\hat{u}}^{min}$+1 possible antenna layouts for the $\hat{u}$th candidate sub-array. The transfer coefficient vector between the $\hat{u}$th candidate sub-array with $\hat{L}_{\hat{u}}$ antennas and the quiet zone can be defined as $\boldsymbol{h}(L_{\hat{u}})$. A matrix composed of the transfer coefficient vectors of all possible layouts of the $\hat{u}$th candidate sub-array can be denoted by $\hat{\mathbf{H}}(\hat{u}) = [\boldsymbol{h}(\hat{L}_{\hat{u}}^{min}), ..., \boldsymbol{h}(\hat{L}_{\hat{u}}^{max})]$. Therefore, by treating the transfer coefficient vector $\boldsymbol{h}(\hat{L}_{\hat{u}})$ of the $\hat{u}$th candidate sub-array with $\hat{L}_{\hat{u}}$ uniformly distributed antennas as an atom in the dictionary, an over-complete dictionary, including $\hat{U}$ candidate sub-arrays, can be expressed in the cell array form: $\xi = \left\{\hat{\mathbf{H}}(1), ..., \hat{\mathbf{H}}(\hat{U})\right\}$. When we calculate the contribution of one candidate sub-array, for example the $\hat{u}$th candidate sub-array, in synthesizing the plane wave field in the following two parts, all possibilities in $\hat{\mathbf{H}}(\hat{u}) = [\boldsymbol{h}(\hat{L}_{\hat{u}}^{min}), ..., \boldsymbol{h}(\hat{L}_{\hat{u}}^{max})]$ should be considered, and the layout with the most significant contribution will be selected.

2) Initial support sub-arrays generation: After constructing the over-complete dictionary, the orthogonal matching pursuit (OMP) algorithm is implemented. By calculating the correlation values between the residual vector and the transfer coefficient vectors of the $\hat{U}$ candidate sub-arrays with all possible numbers of radiators, one can select the sub-array with a certain number of radiating elements which is capable of minimizing the objective function (1) in each iteration. The obtained sub-arrays are referred to as support sub-arrays in the following. After a sub-array with a certain structure is selected, other candidate sub-arrays whose radius differences from the selected sub-array are smaller than the isolation distance r^* are no longer available to avoid the antenna coupling. This procedure is quite similar to that in [10] [19].

3) Backtracking examination: In this part, the support sub-arrays are adjusted individually through the backtracking examination. For each initial support sub-array under examination, a unique optional sub-array region is constructed and is composed of the candidate sub-arrays that will not be coupled with the other support sub-arrays. Combine one possible sub-array in the optional set with the support sub-arrays that are not being examined as a temporary sub-array set. At multiple frequencies, perform the constrained regression calculation for the temporary sub-array set and record the field errors with equation (3). If there is a certain optional sub-array that is more competent in minimizing the average field deviation over the wideband, it will replace the sub-array being examined as the support sub-array. Repeat this procedure for each support sub-array until the wideband field deviation no longer changes.

D. Summary

In the proposed strategies, the over-fitting problem [8] could be significantly relieved with the constrained regression strategy (also with the amplitude-only excitation constraint). Note that $\hat{L}_{\hat{u}}^{max}$ should be restricted to avoid coupling. Actually, in backtracking examination, the possible sub-array can be rotated at multiple angles about the center of PWG for a comprehensive investigation. Though computationally heavy in the design period, the proposed framework effectively generates the ultra-wideband sparse PWG. In application, the PWG can be directly employed with the already obtained excitation codebook at different frequencies.

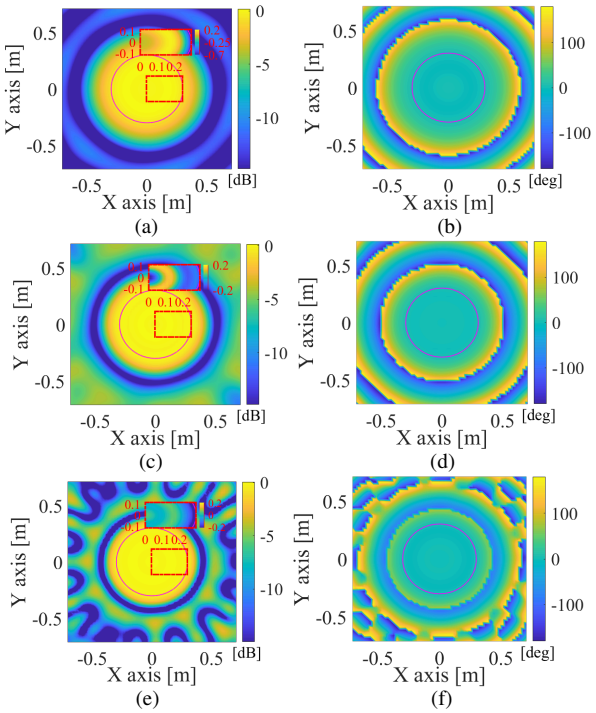

Fig. 2. The amplitude (left) and phase (right) distribution of the synthesized fields across the area with the aperture of D_O. The results are at 2.6 GHz (a,b), 3.5 GHz (c,d), 4.9 GHz (e,f). The purple circle denotes the QZ boundary.

III. Numerical Simulation

In this section, the ultra-wideband performance, ranging from 2.4 GHz to 5 GHz, of synthesizing the desired field in the QZ with our proposed framework is comprehensively investigated. For the dimensions of sampling zones and PWG, the configuration of $D_O = 2m$, $D_Q = 0.6m$, $D_P = 1.2m$, $U = 8$, and $z_0 = 2.1m$, are set to be simulated. $\chi_1 = 1.0$ and 1.7 are used to derive $\hat{L}_{\hat{u}}^{min}$ and $\hat{L}_{\hat{u}}^{max}$. For algorithm implementation, the starting radius, radius interval, and isolation distance are determined as: $\hat{r}_s = 0.5\lambda_b$, $\Delta\hat{r} = 0.1\lambda_b$, and $r^* = 0.5\lambda_b$, respectively. The fields presented are about the main polarization and $\delta_{thr} = -3$ dB. The above settings are adopted for all simulations unless otherwise stated. For comparison, the popular simple least squares method (LSM) is applied to the ABOMP as well, and the complex excitations are therefore employed. Also, the configuration in [11] is used to examine the proposed method.

The generated PWG layout, including 8 sub-arrays and 83 antennas, is shown in Fig. 3, as well as the excitations at different frequencies. With the generated sparse PWG, the fields synthesized at 2.6 GHz, 3.5 GHz, and 5 GHz are shown in Fig. 2. It can be observed that the obtained PWG design is capable of supporting the ultra-wideband plane wave field synthesis, with the maximum peak-to-peak amplitude and phase deviations of 0.89 dB and 7.7°, respectively. Adopting the constrained regression, the maximum undesired field outside

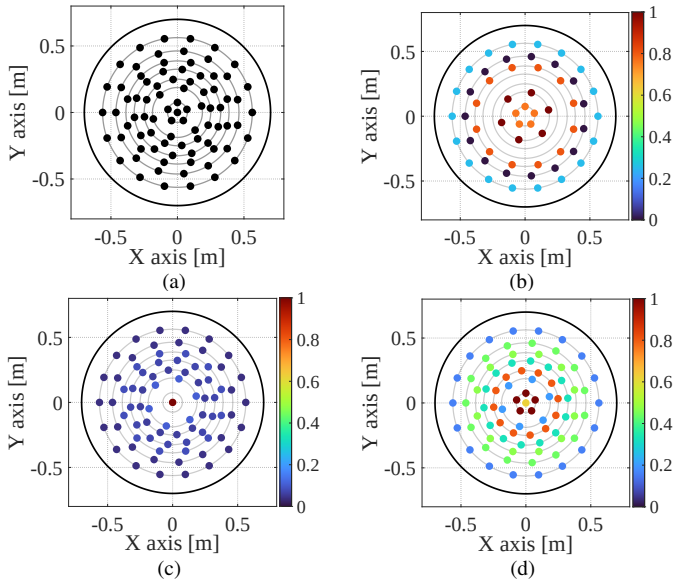

Fig. 3. Layout and excitations of the generated PWG. (a) PWG layout, (b) excitations at 2.6 GHz, (c) excitations at 3.5 GHz, (d) excitations at 4.9 GHz. The color is related to the amplitude-only excitation weight. The sub-arrays with the excitations approaching 0 are not presented.

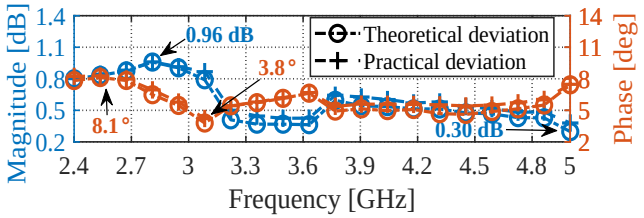

Fig. 4. The comparisons of the theoretical and practical maximum field deviations across the whole QZ at various frequencies points.

the QZ is limited to no more than -3 dB, which is an adequate result in the small anechoic chamber. Over the designed ultra-wideband, the maximum cross-polarized field below -25 dB is achieved, indicating negligible cross-polarization interference.

To evaluate the system robustness, random amplitude and phase noises are considered to be the uniformly distributed random variables, which range from -0.15 dB to 0.15 dB and from -1.5° to 1.5° respectively, and are added to the excitations. Fig. 5 shows the maximum field deviations within the QZ at ultra-wideband frequency points in terms of the theoretical value without excitation noises and the practical value. The practical value is calculated as the average of multiple results of the maximum field deviations excited by the feeding coefficients with noises. It can be observed that the errors most affected by noises are only as low as 0.1 dB in amplitude and 0.8° in phase. In particular, for the two representative frequency points with maximum (0.96 dB, case I) and minimum (0.3 dB, case II) practical amplitude deviations, we perform the simulation test 10000 times as statistically exhibited in Fig. 6. It can be seen that, with the designed PWG system, the amplitude and phase dynamic ranges are effectively limited. With the widely used LSM and the therefore generated PWG, the condition number of the transfer matrix $\mathbf{H}$, however, will be up to 10^7 over the discussed ultra-wideband, resulting in an over-fitting problem.

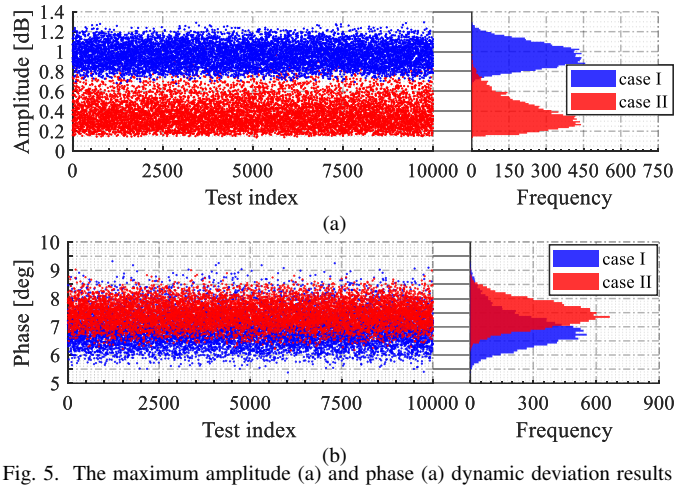

Fig. 5. The maximum amplitude (a) and phase (a) dynamic deviation results from different simulation realizations.

TABLE I
PLANE WAVE SYNTHESIZED WITH VARIOUS CONFIGURATIONS.

PWG configurations	amplitude deviation	phase deviation	RMS deviation	polarization leakage
I: 121 antennas	0.43dB	5.0°	0.0438	−27.6dB
II: 164 antennas	0.78dB	4.9°	0.0339	−26.2dB
III: 192 antennas	0.87dB	9.0°	0.0648	−26dB

It implies that the synthesized field with this PWG system is fragile and unreliable since the high condition number will amplify the unavoidable input errors, such as the uncertainties and quantization errors in the feeding network [8]. In addition, the over-fitting problem makes most of the radiated energy diverge outside the QZ [8] and causes significant multipath reflections in the small chamber, distorting the QZ field.

More PWG configurations, I: $D_Q = 0.7m$, $D_P = 1.4m$, $U = 10$, II: $D_Q = 0.8m$, $D_P = 1.7m$, $U = 11$, and III: $D_Q = 0.9m$, $D_P = 1.7m$, $U = 13$, are further simulated with $\delta_{thr} = -1$ dB. In addition to the maximum field deviations over ultra-wideband, the maximum root mean square (RMS) field deviation is presented as well in Table I. It can be demonstrated that the proposed strategies can be well generalized and extended to various scenarios. In particular, configuration III synthesizes the satisfying plane wave field in the QZ with the same size as in [11], while fewer antennas and excitation channels are required.

IV. Conclusion

This letter presents a novel framework for determining the PWG layout and excitation suitable for ultra-wideband applications. Adopting the amplitude-only excitation method with the sub-array design, the feeding network can be effectively simplified, and the required number of feeding channels is significantly reduced. The simulations of several PWG configurations show that the designed PWG offers adequate and robust plane wave fields within the QZ over 2.4 GHz-5 GHz. Furthermore, the proposed constrained regression strategy could suppress the undesired field outside the QZ, enabling the PWG to be applied to the small anechoic chamber.

REFERENCES

[1] K. Takeda, H. Xu, T. Kim, K. Schober and X. Lin, "Understanding the Heart of the 5G Air Interface: An Overview of Physical Downlink Control Channel for 5G New Radio," *IEEE Commun. Standards Mag.*, vol. 4, no. 3, pp. 22-29, Sep. 2020.

[2] W. Fan et al., "A step toward 5G in 2020: Low-cost OTA performance evaluation of massive MIMO base stations," *IEEE Antennas Propag. Mag.*, vol. 59, no. 1, pp. 38–47, Feb. 2017.

[3] 3GPP TS 38.141-2, 3rd Generation Partnership Project; Technical Specification Group Radio Access Network; NR; Base Station (BS) conformance testing Part 2: Radiated conformance testing, V15.3.0, (2019-09).

[4] P. Kyösti, W. Fan, G. F. Pedersen and M. Latva-Aho, "On Dimensions of OTA Setups for Massive MIMO Base Stations Radiated Testing," *IEEE Access*, vol. 4, pp. 5971-5981, Sep. 2016.

[5] 3GPP TR 37.843, 3rd Generation Partnership Project; Technical Specification Group Radio Access Network; Evolved Universal Terrestrial Radio Access (E-UTRA) and Universal Terrestrial Radio Access (UTRA); Radio Frequency (RF) requirement background for Active Antenna System (AAS) Base Station (BS) radiated requirements, V15.5.0, (2019-09).

[6] A. Buonanno, M. D'Urso, and G. Prisco, "Reducing complexity in indoor array testing," *IEEE Trans. Antennas Propag.*, vol. 58, no. 8, pp. 2781–2784, Aug. 2010.

[7] H. Wang, W. Wang, H. Gao, Y. Wu, Y. Liu, and J. Gao, "Plane wave compensation technique for multiple-input multiple-output over-the-air testing in small multi-probe anechoic chamber," *IET Microw., Antennas Propag.*, vol. 13, no. 15, pp. 2625–2631, Dec. 2019.

[8] Z. Yang, Z. Wang, Y. Zhang and S. Gao, "Robust Plane Wave Generator Design in Small Anechoic Chamber Setup Using Parameterized Field Method," *IEEE Access*, vol. 8, pp. 187052-187059, Oct. 2020.

[9] O. M. Bucci, M. D. Migliore, G. Panariello, and D. Pinchera, "Plane wave generator: Design guidelines, achievable performances and effective synthesis," *IEEE Trans. Antennas Propag.*, vol. 61, no. 4, pp. 2005–2018, Apr. 2013.

[10] Y. Li, L. Gao, H. Sun and X. Zhang, "Plane-Wave Synthesis: A Sparse Representation Perspective," *IEEE Antennas Wireless Propag. Lett.*, vol. 19, no. 9, pp. 1644-1648, Sep. 2020.

[11] Y. Zhang, Z. Wang, X. Sun, Z. Qiao, W. Fan and J. Miao, "Design and Implementation of a Wideband Dual-Polarized Plane Wave Generator With Tapered Feeding Nonuniform Array," *IEEE Antennas Wireless Propag. Lett.*, vol. 19, no. 11, pp. 1988-1992, Nov. 2020.

[12] F. Scattone, D. Sekuljica, A. Giacomini, F. Saccardi, J. Acree, J. Estrada, and L. J. Foged, "Dual polarized plane wave generator design for direct far-field testing," in *Proc. IEEE Int. Symp. Antennas Propag. USNC-URSI Radio Sci. Meeting*, pp. 1–4, Jul. 2019.

[13] D. Pinchera, M. D. Migliore, F. Schettino, M. Lucido, and G. Panariello, "An effective compressed-sensing inspired deterministic algorithm for sparse array synthesis," *IEEE Trans. Antennas Propag.*, vol. 66, no. 1, pp. 149–159, Jan. 2018.

[14] M. A. Abdelhay, N. O. Korany, and S. E. El-Khamy, "Synthesis of uniformly weighted sparse concentric ring arrays based on off-grid compressive sensing framework," *IEEE Antennas Wireless Propag. Lett.*, vol. 20, no. 4, pp. 448–452, 2021.

[15] A. Massa, P. Rocca, and G. Oliveri, "Compressive sensing in electromagnetics—A review," *IEEE Antennas Propag. Mag.*, vol. 57, no. 1, pp. 224–238, Feb. 2015.

[16] V. Rodriguez, "Basic rules for indoor anechoic chamber design," *IEEE Antennas Propag. Mag.*, vol. 58, no. 6, pp. 82–93, Dec. 2016.

[17] D. Cheng and C. Chen, "Optimum element spacings for Yagi-Uda arrays," *IEEE Trans. Antennas Propag.*, vol. AP-21, no. 5, pp. 615–623, Sep. 1973.

[18] S. Boyd and L. Vandenberghe, *Convex Optimization.* Cambridge, U.K.: Cambridge Univ. Press, 2004.

[19] H. Wang, W. Wang, Y. Wu, B. Tang, W. Zhang and Y. Liu, "Probe Selection for 5G Massive MIMO Base Station Over-the-Air Testing," *IEEE Antennas Wireless Propag.* Lett., vol. 19, no. 11, pp. 1998-2002, Nov. 2020.